Increasing chemical weathering in the Himalayan system since the Last Glacial Maximum

Maarten Lupker, Christian France-Lanord, Valier Galy, Jérôme Lavé, Hermann Kudrass

Increasing chemical weathering in the Himalayan system since the Last Glacial Maximum

*Maarten LUPKER[1] *, Christian FRANCE-LANORD[1], Valier GALY[2], Jérôme LAVÉ[1], Hermann KUDRASS[3]*

[1] Centre de Recherches Pétrographiques et Géochimiques (CRPG), UMR 7358, CNRS-Université de Lorraine, 15 rue Notre Dame des Pauvres, 54501 Vandoeuvre les Nancy, Cedex, France.

[2] Woods Hole Oceanographic Institution (WHOI) – Department of Marine Chemistry and Geochemistry, 360 Woods Hole Rd., Woods Hole, MA 02543, USA.

[3] MARUM zentrum für Marine Umweltwissenschaften, Bremen, Germany.

*Corresponding author:

Maarten Lupker

IGP-ETHZ - NW C 85 - Clausiusstrasse 25, 8092 Zürich - Switzerland

+41 446329383

maarten.lupker@erdw.ethz.ch

ABSTRACT:

Continental chemical weathering is central in Earth's surface biogeochemical cycles as it redistributes elements across reservoirs such as the crust and the oceans. However the evolution of weathering through time and its response to external forcing such as changes in climate remain poorly constrained. In this work, a composite sediment record from the Bay of Bengal is used to document the evolution of chemical weathering in the Himalayan system (Himalayan range and Indo-Gangetic floodplain), the world largest sediment conveyor to the oceans, since the Last Glacial Maximum (LGM). The degree of weathering of the sediments is documented using mobile to immobile ratios such as K/Si and H_2O^+/Si as well as detrital calcite abundance. Robust weathering proxies are derived by correcting the chemical composition of sediment for sorting effects that occur during transport and deposition. The Bay of Bengal record is also further compared to the chemical composition of modern river sediments from the Ganga & Brahmaputra basin. Weathering proxies all indicate that the sediments exported by the Ganga & Brahmaputra Rivers became increasingly weathered over the past ~21 kyr, whereas, Sr, Nd and major elements suggest a constant sediment provenance in the system over the last 21 kyr. These changes in the degree of weathering of the sediments show that the weathering flux exported by the system to the Indian Ocean during the LGM was significantly lower than at present and demonstrate that chemical weathering in continental scale basins such as the Ganga & Brahmaputra responds to Late Quaternary climate changes.

1. Introduction:

Chemical weathering of continental rocks is the main source of soluble elements to the oceans and therefore exerts a first order control on oceanic bio-geochemical cycles. Over geologic time scales, silicate weathering and subsequent carbonate precipitation also draws down atmospheric CO_2 thereby stabilizing the earth's climate (Walker et al., 1981). Continental weathering fluxes are a function of continent lithology, tectonic activity and climate but the mechanisms and feedbacks linking silicate weathering to the earth's climate remain debated (France-Lanord and Derry, 1997; Willenbring and von Blanckenburg, 2011). A better understanding of these complex climate-weathering couplings can be gained by studying the response of continents to climatic transitions in the past.

The role of the Himalayan orogeny in the long-term forcing of oceanic cycles and the global climate has retained much attention (France-Lanord and Derry, 1997; Raymo et al., 1988). However, the temporal variability of and controls on the evolution of weathering fluxes exported by large basins remains poorly constrained and is often difficult to reconstruct (Limmer et al., 2012). In particular, direct characterization of the response of chemical weathering to abrupt climate perturbations has heretofore remained a challenge. We present a record of chemical weathering intensity in the Himalayan system since the LGM. The Himalayan system is defined here as the Himalayan range and the downstream Indo-Gangetic floodplain drained by Ganga and Brahmaputra Rivers. No major change in tectonic forcing of the Himalayan orogeny has been documented so far over the last glacial-interglacial period, which enables us to discuss variations in sediment weathering as a response to climate change.

2. Setting and methods:

47

48 The central part of the Himalayan range is drained by two major rivers, the Ganga and
49 Brahmaputra (Figure 1). Currently, the Ganga & Brahmaputra transfers ca. 1.10^9 Mt of
50 sediments to the Bay of Bengal, of which 90% is transported during the monsoon (RSP,
51 1996). River sediments were sampled mainly during monsoon seasons, in 2002, 2004, 2005,
52 2007, 2008 and 2010 across the Indo-Gangetic floodplain. Sampling locations mainly
53 included the front of the Himalayan range for the main trans-Himalayan Rivers of the Ganga
54 & Brahmaputra system, the outlet of the Ganga and the Brahmaputra as well as their
55 confluence - the lower Meghna - which integrates the entire sediment load exported from the
56 Ganga & Brahmaputra basin (Figure 1). When possible, sediments were sampled along
57 vertical depth profiles through the water column in order to capture the full variability of the
58 sediment load. These profiles were complemented by bedload samples dredged from the
59 active channel of the rivers and freshly exposed bar sediments. Details on the sampling
60 procedure are described in Lupker et al. (2011).

61 Sediment cores were retrieved during RV *Sonne* cruise SO93 in 1994 from the shelf
62 (105KL and 107KL) and the active channel levee system of the middle fan (117KL, 118KL
63 and 120KL) (Ittekkot et al., 2003). The chronology of the cores is provided by re-calibrated
64 (Reimer et al., 2009) ^{14}C ages on planktonic foraminifers (Weber et al., 1997) as well as
65 ^{137}Cs, ^{210}Pb and ^{228}Ra gamma spectrometry (Michels et al., 1998). Scarce hemipelagic layers
66 were excluded from the study in order to focus on turbiditic sediments representing the Ganga
67 & Brahmaputra detrital signal (Pierson-Wickmann et al., 2001; Weber et al., 1997). We
68 interpret our data by constructing a composite Log from the shelf and levees core following
69 the approach detailed in Galy et al. (2008).

70 River suspended river sediments were filtered through 0.22 µm PES membrane filters
71 within 24 h of sampling and dried in the lab. Major element concentration was determined by

ICP-OES after $LiBO_2$ fusion at SARM, Nancy – France (Carignan et al., 2001). Core samples were repeatedly rinsed with water in order to remove salt contributions. Nevertheless, Na was not considered in this study due to seawater contamination even after these rinsing steps. Carbonate contents were measured manometrically from the CO_2 released after reaction with H_3PO_4 and the evolved CO_2 was subsequently analyzed for C and O isotopic composition (Galy et al., 1999). Sr and Nd isotopic compositions were measured on the acid leached, silicate fraction of the river and core sediments by TIMS after classical separation and purification by ion exchange resins. Sediment hydration [H_2O^+] and isotopic composition δD-SMOW was measured by EA-IRMS after degassing the samples to remove adsorbed free-water (Lupker et al., 2012b). The long-term reproducibility is better than 0.1 H_2O^+ wt % and 2 ‰ δD-SMOW.

3. Sediment sorting effects on the chemical composition of detrital sediments:

3.1 Hydrodynamic control of sediment sorting

The chemical composition of river sediments has to be interpreted carefully. Sediment vertical depth profiles recovered from the water column of large rivers show a strong heterogeneity in terms of concentration and chemical composition. These heterogeneities are the result of the hydrodynamic sorting of sediments, based on grain-size, shape and density, which induce mineralogical and thus chemical differentiation of sediments within the water column (Bouchez et al., 2011a; Bouchez et al., 2011b; Garzanti et al., 2011; Lupker et al., 2011; Singh and France-Lanord, 2002a). The mineralogy of sediments from the Himalayan system is dominated by quartz, micas and feldspar, with occurrences of other phyllosilicates, clay assemblages and hydroxides in the finer fraction (Garzanti et al., 2011; Garzanti et al., 2010). These minerals are segregated during sediment transport: coarse-grained quartz is

97 enriched in the bedload and at the bottom of the water column while phyllosilicates such as
98 micas and clays are comparatively enriched in the shallow surface waters of the river, leading
99 to a strong contrast in chemical composition between samples of a single reach. This is best
100 illustrated using the immobile element ratios Fe/Si and Al/Si (Figure 2). Fe, Al and Si are, to
101 a first order, immobile elements during Himalayan erosion and are thus not notably affected
102 by chemical weathering (Galy and France-Lanord, 2001). The sediments sampled across the
103 Indo-Gangetic plain form a unique mixing trend (to the exception of a few bedload samples
104 that are enriched in Fe due to heavy mineral placer effects) between quartz rich (low Al/Si
105 and Fe/Si) bottom sediments and clay rich (high Al/Si and Fe/Si) surface sediments. Al/Si and
106 Fe/Si are directly correlated to the bulk sediment grain-size and are a proxy of mineral sorting
107 (Bouchez et al., 2011a; Lupker et al., 2011). A single sediment sample from a given river
108 reach can therefore not be considered, a priori, as representative of the whole sediment load,
109 its chemical composition being dependent on river hydrodynamics at the moment of
110 sampling.
111
112 *3.2 Weathering proxies in modern river sediments*
113
114 The degree of chemical weathering experienced by sediments in the Himalayan
115 system can be traced from detrital sediments by using the mobile to immobile elemental ratios
116 of river sediments such as K/Si and H_2O^+/Si. The structural hydroxyl content of sediments,
117 H_2O^+, is a proxy of chemical weathering that traces mineral hydrolysis and secondary neo-
118 formations (Lupker et al., 2012b). Sediment sorting effects also apply to mobile elements
119 such as K and H_2O^+. The K/Si and H_2O^+/Si ratios are dominantly controlled by the grain size
120 of the sediments, i.e. clay to quartz mixing (Lupker et al., 2012b) and are, to a first order,
121 linearly correlated to their Al/Si ratio as shown by Figure 3, where these ratios are plotted for

sediments from the modern Himalayan system. By using a sediment depth profile sampling approach on modern rivers, we characterize these sorting effects as this method allows sampling a full set of sediments covering a wide range of grain sizes. The degree of chemical weathering can then be assessed based on the trend formed by the chemical composition of the sediments in diagrams such as Figure 3, this trend being representative of the entire sediment load exported by the considered river.

In addition to silicate weathering proxies, we determined the calcite content and the Ca/Si ratio in Bay of Bengal sediments that reflects the carbonate weathering intensity in the Himalayan system. Carbonates, including calcite, account for over 80 % of the bulk Ca and Ca/Si therefore mainly reflects carbonate content. Both carbonates and Ca content are not grain size dependent (Lupker et al., 2011) and are therefore not corrected for sediment sorting.

3.3 Accounting for sediment sorting effects in detrital records

For detrital records such as the Bay of Bengal cores, changes in sediment transport and deposition patterns induce changes in the grain size of deposited sediments that, in turn, affect the chemical composition of the record. Hence, sediment sorting also has to be taken into account in order to compare the degree of weathering of samples with variable grain-sizes (variable Al/Si ratios). However, unlike for modern rivers, it is not possible for a given age interval of the record to recover a set of sediment samples spanning different grain sizes that would fully describe the sediment weathering trend. By considering that each sample of the Bay of Bengal record is the result of the mixing between a coarse-grained end-member, similar to bedload material and a fine-grained, clay rich sediment, it is nevertheless possible

146 to normalize mobile to immobile ratios (X/Si) to a common Al/Si composition as illustrated
147 in Figure 4 and equation 1:

$$\frac{X^*}{Si} = \frac{\overline{Al}}{Si} \cdot A + B \quad (1)$$

148

149 where A and B are respectively the slope and intercept of the linear regression through the
150 sample and coarse grained end-member composition (Figure 4). Such normalized ratios allow
151 comparing the chemical composition of sediments that have contrasted grain sizes, while
152 properly accounting for sorting effects. Doing so, we assume that a unique coarse-grained
153 end-member composition can be assigned to the low Al/Si mixing end-member and that the
154 weathering signature is mainly carried by the small grain size, clay fraction of the sediment
155 load. This is a reasonable approximation as: 1) contrary to the fine grained suspended load, no
156 systematic evolution of K/Si and H_2O^+/Si ratios of modern bedloads in the Ganga basin is
157 detected from up to downstream (Lupker et al., 2012b), suggesting that the effect of chemical
158 weathering during transfer in the floodplain is negligible for the coarse fraction of the
159 transported sediments, and 2) the transfer time of bedload material is thought to be an order of
160 magnitude longer than that of fine-grained suspended load (Granet et al., 2010), which makes
161 it less sensitive than the suspended load to short-term upstream variations.

162 All corrected ratios presented here were normalized to a common Al/Si value of 0.23.
163 They are referred to as X/Si* and are listed in the supplementary information along with the
164 composition of the coarse grained end-member used in the calculations. The Al/Si value of
165 0.23 was chosen as the average composition of the sediments exported by the modern Ganga,
166 which was determined by modeling the chemical composition of sediments as a function of
167 the river's hydrological conditions and integrated over a 25-year average hydrograph (Lupker
168 et al., 2011). This composition is also close to the composition of the Himalayan crust eroded
169 in the Ganga basin (Lupker et al., 2011). It should be noted that the choice of the Al/Si ratio
170 used for normalizing K/Si and H_2O^+/Si ratios only determines the absolute values of K/Si*

and H_2O^+/Si* but has no influence on the general trends observed for Bay of Bengal sediments.

Before normalization, the raw K/Si and H_2O^+/Si ratios of sediments from the Bay of Bengal cores are correlated to Al/Si (Figure 5), which supports that K/Si and H_2O^+/Si are dominantly controlled by grain size and sorting effects. However the normalized K/Si* and H_2O^+/Si* ratios show no correlation with Al/Si, which suggests that our normalization properly accounts for sediment sorting.

3.4 Comparison with modern river sediments

In order to compare the weathering degree of the Bay of Bengal sediment record to modern river sediments we applied a similar normalization to the river sediments. The average compositions of modern river sediments for elements prone to sorting effects (K/Si*, H_2O^+/Si*), reported in Figure 5, were determined by evaluating the regression through all available data of each river reach and a coarse-grained end-member at Al/Si = 0.23. The Himalayan front end-member was reconstructed from the river sediments sampled at the Himalayan front in the Ganga basin and the Brahmaputra basin separately assuming that ca. 60% of the total sediment flux exported to the Bay of Bengal come from the Brahmaputra and the remaining 40 % come from the Ganga basin (RSP, 1996). For compositions that are not affected by sorting effects (calcite, Ca/Si, $^{87}Sr/^{86}Sr$, εNd, $\delta^{18}O$ and $\delta^{13}C$), a simple average for the Ganga, Brahmaputra and lower Meghna and a weighted mean for the Himalayan front were considered (details can be found in supplementary information and Table S2).

4. Weathering in the Himalayan system:

4.1 Weathering in the modern system

196

197 Chemical weathering is marked by a change in the mobile to immobile ratio at
198 constant Al/Si ratio. This mobile element depletion is highest for fine-grained (high Al/Si)
199 sediments (Figure 3). Modern Himalayan rivers sediments, sampled at the front of the range
200 show high K/Si ratios and low H_2O^+/Si ratios compared to the sediments sampled at the outlet
201 of the Ganga & Brahmaputra basins and their confluence, the lower Meghna (Figure 3). The
202 loss of K and gain in hydration during floodplain transfer marks the weathering of the
203 sediments within the floodplain. Even if part of this weathering signal may stem from the
204 sediment contribution of the southern (Ganga) and eastern (Brahmaputra) tributaries, their
205 sediment fluxes remain small compared to that of Himalayan tributaries (Lupker et al., 2012b;
206 Singh and France-Lanord, 2002a). Calcite weathering in the modern floodplain is significant
207 and leads to almost complete dissolution in Brahmaputra sediments in Bangladesh (Singh and
208 France-Lanord, 2002a; Singh et al., 2005) while modern Ganga sediments in Bangladesh
209 display a low calcite content of ca. 3 wt% (Lupker et al., 2012b).

210 It has been shown that in the modern Ganga basin, weathering within the floodplain
211 outweighs weathering within the Himalayan range (Lupker et al., 2012b; West et al., 2002).
212 Significant K depletion and H_2O^+ gain is only recorded when sediments transit through the
213 floodplain (Lupker et al., 2012b), which is attributed to the longer residence time of sediments
214 in the floodplain than in the Himalayan range. Overall, these observations emphasize the
215 strong floodplain control on weathering in the Himalayan system.

216

217 *4.2 Weathering record of the Bay of Bengal:*

218

219 The normalized weathering indexes (K/Si* and H_2O^+/Si*) are not biased by sorting
220 effects and can thus be applied to the Bay of Bengal record to reconstruct temporal variations

in chemical weathering. Composite logs of K/Si* and H_2O^+/Si* (Figure 6) show a progressive evolution towards lower K/Si* and higher H_2O^+/Si* ratios from the LGM to present. Both weathering proxies suggest that during the LGM, sediments exported to the Bay of Bengal were less weathered than recent Bay of Bengal and modern lower-Meghna sediments. It should also be noted that the chemical composition of sediments from the most recent part of the Bay of Bengal record agrees well with that of the sediments currently exported by the lower Meghna (Figure 6).

Calcite content and Ca/Si ratios also decrease from LGM to present (Figure 6). Calcite in sediments from the Bay of Bengal is of detrital origin as demonstrated by their isotopic composition ($\delta^{18}O_{PDB}$ ranging from -15 to -6 ‰, see electronic appendix), much lower than marine biogenic calcite (Hoehndorf et al., 2003) and within the range of composition of detrital Himalayan river calcite (Lupker et al., 2012b). The decrease in calcite concentration and Ca/Si ratios since the last glacial maximum supplement the K/Si* and H_2O^+/Si* records, further reinforcing the conclusion that sediment weathering increased during the studied period.

Estuarine and early digenetic reactions such as weathering and reverse weathering may affect the composition of deposited sediments (Jones et al., 2012; Michalopoulos and Aller, 1995; Michalopoulos and Aller, 2004; Wallmann et al., 2008). The close agreement between the chemical composition of modern lower Meghna sediments and the recent part of the record, both from the shelf and the levee, suggests that estuarine processes do not alter significantly the composition of river sediments delivered to the Bay of Bengal. The chemical weathering of sediments after deposition cannot explain the trends observed in the Bay of Bengal record either. Indeed, post-depositional weathering would lead to down-core increase in the weathering intensity which is opposite to the observed trend. Reverse weathering leads to an uptake of K and to an overall decrease in structural OH radicals of the sediments

(Michalopoulos and Aller, 1995) but cannot explain the observed down-core increase in detrital carbonate content. Furthermore, during reverse weathering reactions, the newly formed minerals will form in equilibrium with seawater so that the D/H isotopic composition of their hydroxyls groups should become heavier as reverse weathering reactions proceed. However no systematic down-core increase in δD_{H2O+} is observed (supplementary information, Figure S1).

5. Sediment provenance since the LGM:

Potential sediment source effects on the chemical composition of Bay of Bengal sediments since the LGM must be taken into account as changes in precipitation and erosion patterns within and across the Himalayan range may have affected the sedimentary record. The Sr and Nd isotopic signatures of river sediments in the Himalayan range are a first order indicator of the erosion balance between the Lesser Himalaya (LH) and High Himalaya (HHC) (and Transhimalayan formations – THB – for Brahmaputra) as these units have contrasted isotopic compositions (France-Lanord et al., 1993; Singh and France-Lanord, 2002a). Sediments from the Ganga and Brahmaputra basins also show distinctive Sr and Nd isotopic compositions so that changes in the balance of sediment supply from both basins would be detected (Figure 7).

Previous studies have shown contrasting changes in the balance between sediments from the LH and HHC in the Indus basin (Clift et al., 2008) and the western part of the Ganga basin (Rahaman et al., 2009; Rahaman et al., 2010; Srivastava and Shukla, 2010) since deglaciation. However, both Sr and Nd isotopic compositions of Bay of Bengal sediments appear constant, implying that there is no evidence for major changes in the distribution of erosion within the Himalayan range at this scale (Figure 7). The Sr and Nd record also

suggests that the balance between the Brahmaputra and Ganga has remained roughly constant over the last 20 kyrs. A significant change in the sediment balance between Ganga and Brahmaputra would furthermore result in a correlated evolution of K/Si* and H_2O^+/Si*, whereas these ratios are actually anti-correlated since the LGM (Figure 6), demonstrating that the weathering signal overprints any potential change in sediment source.

An increase in sediments from the Siwalik or from southern tributaries through time is also very unlikely. Siwalik rocks and sediments are characterized by high carbonate content and low $\delta^{13}C$ compositions (Lupker et al., 2012b; Sanyal et al., 2005). Thus, the concomitant decrease of both carbonate content and $\delta^{13}C$ values observed in the Bay of Bengal sediments is not compatible with an increase of sediment supply from the Siwaliks. In addition, sediments from the Chambal River in the Ganga basin and the Eastern tributaries of the Brahmaputra basin (Lohit and Dibang) have distinctively higher Fe/Si ratios and unradiogenic Sr and Nd signatures (Lupker et al., 2012b; Singh and France-Lanord, 2002a; Singh et al., 2008) that are not identified in our record (see supplementary information, Figure S1).

Altogether, the observed changes in Bay of Bengal sediment mobile elements composition since the LGM can thus be primarily attributed to changes in the chemical weathering intensity in the Ganga & Brahmaputra basin.

6. Discussion:

6.1 Climatic forcing of Himalayan chemical weathering

During the last 21 kyrs, climate has been the main external forcing of Himalayan erosion that could have affected the Bay of Bengal weathering signal. Paleo-temperature reconstructions over the Himalayan system are scarce but indicate a ca. 2 °C colder LGM sea

296 surface temperature (SST) in the Bay of Bengal (Kudrass et al., 2001). Hydrological changes
297 were significant with strongly reduced monsoon and therefore a lower continental runoff
298 during the last glacial (Cullen, 1981; Duplessy, 1982; Herzschuh, 2006; Kudrass et al., 2001),
299 which reduced the sediment supply to the Bay of Bengal (Goodbred, 2003; Weber et al.,
300 1997). Precipitation and temperature directly control the weathering rate of minerals (White
301 and Blum, 1995), and the conditions during the LGM where therefore less favorable for
302 intense weathering in the floodplain. These changes in floodplain weathering are confirmed
303 by the evolution of clay assemblages in the southern part of the basin that suggests an
304 increase in weathering intensity from at least 10 kyr to present (Heroy et al., 2003).
305 Additional, independent processes should not be excluded (Blum and Tornqvist,
306 2000). The lower base level and a reduced sediment supply during the LGM could have lead
307 to channel incision and a narrower active floodplain (Goodbred, 2003; Heroy et al., 2003),
308 which would reduce channel – floodplain interactions and limit the supply of weathered
309 floodplain sediments to the Bay of Bengal. A complete abandonment of the floodplain during
310 the LGM is nevertheless unlikely as floodplain derived organic material is persistent in the
311 Bay of Bengal cores throughout the deglaciation (Galy et al., 2008) but changes in the
312 sediment locus and volume being mobilized should not be excluded (Dosseto et al., 2010).
313 The weathering degree of sediments does, however, not show any clear change in
314 response to the decrease of monsoon intensity after the Holocene Climatic Optimum (HCO)
315 (Kudrass et al., 2001). The sediment fluxes during the HCO were up to double modern fluxes
316 as indicated by sediment volume reconstructions (Goodbred, 2003). These high sediment
317 fluxes may have obliterated the intense weathering conditions prevailing at that time. It can
318 also not be ruled out that modern sediments reflect the export of material weathered during
319 the HCO owing to a long-sediment transfer time so that the post-HCO decrease in
320 precipitation is not yet recorded in the Bay of Bengal. The impact of anthropogenic activity in

the Indo-Gangetic floodplain should also be considered as intense land use changes, certainly significant more than 3 centuries ago (Ramankutty and Foley, 1999), may overprint the climatic forcing of the weathering degree in the recent part of the record if already significant thousands of years ago (Bayon et al., 2012).

The sediment transfer time through the Himalayan system has to be considered as well, as a long transfer time would induce a temporal offset between the suggested climatic forcing of weathering in the Ganga & Brahmaputra basin and its recording in the sediment record of the Bay of Bengal. The sediment transfer time in large continental basins remains difficult to constrain. U-series disequilibrium studies on Ganga sediments suggest that the transfer time of coarse sediments may reach several 100 kyrs while fine grained suspended material travel in less than 25 kyrs (Chabaux et al., 2009; Chabaux et al., 2006; Granet et al., 2010; Granet et al., 2007). However, simple mass balance considerations based on the volume of the active floodplain and grain size along with modern sediment fluxes suggest shorter transfer time scales of 1 kyrs for fine (<100 μm) sediments along the Ganga floodplain (Lupker et al., 2012a) and most probably even shorter transfer time along the narrower Brahmaputra floodplain. In addition, short term variability of the chemical composition of Ganga sediments observed in Bangladesh and attributed to the variable input of a > 1000 km distant, upstream tributary suggests that for fine-grained suspended sediment the transfer time can be of the order of the season (Lupker et al., 2012b). Finally, a relatively short transfer time is also supported by the organic carbon Bay of Bengal record, which shows a change in vegetation photosynthetic type over the Ganga & Brahmaputra basin from the last glacial to present (Galy et al., 2008). This vegetation change follows the model predictions and would not be recorded if the sediment transfer time exceeded glacial – interglacial time scales.

Although the transfer time of sediments is probably significant and remains difficult to

quantify, a network of evidences suggests that it is lower than glacial-interglacial time scales for fine sediments such as those composing the Bay of Bengal record (high Al/Si ratios). Thus, the observed weathering trends most likely results from the direct or indirect climatic forcing of weathering in the Ganga & Brahmaputra basin.

6.2 Towards a quantitative weathering budget

Changes in the net weathering flux or dissolved flux (φ_X) can be estimated by considering that, at steady state, the weathering flux exported as solutes to the oceans is the product of the mobile element depletion of sediments (ΔX) and the sediment flux (F_{sed}) (Lupker et al., 2012b):

$$\varphi_X = F_{sed} \cdot \Delta X = F_{sed} \cdot \left(\frac{\overline{X}}{\overline{Si}_{Source}} \cdot \overline{[Si]}_{Source} - \frac{\overline{X}}{\overline{Si}_{Sink}} \cdot \overline{[Si]}_{Sink} \right) \quad (2)$$

Where $\overline{X/Si}$ is the average mobile to immobile ratio of the source and sink sediments and $\overline{[Si]}$ the average Si concentration of the sediments. A high-resolution reconstruction of weathering fluxes is pointless, as the steady state hypothesis is likely not fully satisfied over short time-scales because of late Holocene climatic variations and anthropogenic imprints (possibly acting over timescales shorter than the sediment residence time in the floodplain). A first order estimate can nevertheless be made by comparing the loss of K, and gain in H_2O^+, relative to Himalayan front sediments for the LGM (19 – 22 kyr) and the modern (0 – 2 kyr) part of the record.

The average $\overline{K/Si}$ and $\overline{H_2O^+/Si}$ ratios of the exported sediment flux can be estimated based on the average Al/Si ratio of the sediments, as Al/Si is relatively insensitive to chemical weathering. The average Al/Si ratio of sediments was estimated to be 0.23 for the Ganga in Bangladesh (Lupker et al., 2011). Hence, $\overline{K/Si}$ and $\overline{H_2O^+/Si}$ are well

approximated by $\overline{K/Si^*}$ and $\overline{H_2O^+/Si^*}$, as for these ratios the composition of the sediment is normalized to an Al/Si ratio of 0.23.

Because the effect of weathering in the Himalayan range is not detected on the K/Si and H_2O^+/Si composition of modern river sediments sampled at the front of the Himalayan range (Lupker et al., 2012b), we conclude that the composition of these sediments is a good approximation of the average composition of the sediment source. This observation also excludes the possibility of a significantly lower degree of sediment weathering within the Himalayan range during the LGM, as weathering for K and H_2O^+ is already limited at present. We therefore consider that the Himalayan front end-member (as constrained from the mixture of 60 % of sediments from the Himalayan front in the Brahmaputra basin and 40 % in the Ganga basin) is a good first order approximation of the sediment source composition, both in the modern day system and during the LGM. The modern dissolved flux of Si is negligible compared to the solid Si fluxes (Galy and France-Lanord, 2001) and this was most likely also the case during the LGM as the chemical weathering intensity was even lower than at present. Furthermore the Si concentration of the exported sediments is only slightly affected by sequestration of Si-rich bedload sediments in the modern floodplain (Lupker et al., 2012b) and we make the assumption that this has been true during the last 21 kyrs. Hence, we consider $\overline{[Si]}$ constant during the time span of our record.

The change in the weathering flux ($R\varphi_X$) of mobile element X from LGM to present relative to the modern fluxes can therefore be written as:

$$R\varphi_X = \frac{\varphi_X|_{Modern} - \varphi_X|_{LGM}}{\varphi_X|_{Modern}} = \frac{F_{Sed}^{Modern} \cdot \left(X/Si^*|_{HimalFront}^{Modern} - X/Si^*|_{BoB}^{Modern} \right) - F_{Sed}^{LGM} \cdot \left(X/Si^*|_{HimalFront}^{LGM} - X/Si^*|_{BoB}^{LGM} \right)}{F_{Sed}^{Modern} \cdot \left(X/Si^*|_{HimalFront}^{Modern} - X/Si^*|_{BoB}^{Modern} \right)} \quad (3)$$

In order to estimate $R\varphi_X$ from eq. 3, the sediment flux (F_{sed}) has to be estimated at present and during the LGM. Based on extensive gauging data the combined modern flux of the Ganga & Brahmaputra in Bangladesh is estimated to be ca. 1.10^9 $t.yr^{-1}$ (RSP, 1996). The past sediment flux exported by the Ganga & Brahmaputra is largely unknown. However, qualitatively, the sediment flux was most probably lower during the LGM than at present. A weakened monsoon during the LGM (Kudrass et al., 2001; Sharma et al., 2004) may have limited physical erosion in the Himalayan range and lowered the transport capacity of the rivers, leading to a lower sediment flux to the Bay of Bengal (Weber et al., 1997; Goodbred, 2003). A very conservative estimate of the minimum value of $R\varphi_X$ can therefore be made assuming a constant sediment flux over the period. By doing so we also isolate the effect of the change in the chemical composition of sediments only.

$R\varphi$ was computed using eq. 3 for K and H_2O^+ and is summarized in Table 1. Uncertainties on the K/Si* and H_2O^+/Si* ratios of individual samples are ca 3% (supplementary information S3). This is of the same order as the variability of K/Si* and H_2O^+/Si* ratios over the 0 – 2 and 19-22 kyr intervals or of the uncertainties on the regression through the data for the Himalayan front sediments. These uncertainties were propagated through the calculations of $R\varphi_X$ and reported in Table 1. The sensitivity of the weathering budget to the average Al/Si ratio of sediments is lower than the uncertainty propagated from the variability of K/Si* and H_2O^+/Si* ratios (see supplementary information S3). This first order estimation shows that the weathering flux during the LGM was at least 67 (±28) and 89 (±36) % lower (for K and H_2O^+, respectively) than for the modern period (0-2 kyrs) for a constant sediment flux. The main uncertainty on these estimates comes from the uncertainty on the sediment Ganga and Brahmaputra sediment flux during the LGM. A sediment flux during the LGM of half the present day sediment flux would induce a 83 and 95 % lower weathering flux during the LGM compared to present for K and H_2O^+, respectively.

The loss of K in the Himalayan system is mainly attributed to the weathering of biotite while the gain in hydration also depends on clay secondary mineral formation (Lupker et al., 2012). Because the reaction mechanisms in both cases are different, their sensitivity to changes in precipitation and temperature is also most probably different. Despite our estimates for both proxies being similar within uncertainty, it would not be surprising that the relative changes in weathering fluxes recorded by K and H_2O^+ could be different. It is not possible to estimate the relative change in calcite weathering using a similar approach, because for calcite the Himalayan source composition cannot be reliably estimated. Indeed, significant carbonate dissolution has been documented within the Himalayan range (Galy and France-Lanord, 1999), hence, Himalayan front river sediments cannot accurately represent the eroded source. In addition, no direct estimation of the average calcite content of Himalayan rocks is available.

Our quantification of the change in the net weathering flux from LGM to present should only be considered as a rough estimate. In particular, it should be kept in mind that these estimates somewhat depend upon the assumption of a transition between two steady state weathering stages. Nevertheless, our estimates suggest that changes in weathering fluxes exported by the Himalayan system have been significant over short time scales of ca. 20 kyrs. The magnitude of the variations in weathering fluxes reconstructed here exceeds previous estimates (Foster and Vance, 2006). This may be attributed in part to the very high weathering rates of glacial outwash during the very early stage of an interglacial, as proposed earlier (Foster and Vance, 2006; Vance et al., 2009) combined to the short time span of our record. However, for the Himalayan system the weathering intensity in the modern floodplain (Lupker et al., 2012b; West et al., 2002) supports the dominant role of the floodplain in modulating glacial to interglacial weathering fluxes. This study further emphasizes that

present day weathering rates are likely higher than long-term averages, which supports the idea that the imbalance of oceanic geochemical cycles may at least partially derive from the over-estimation of Quaternary riverine fluxes to the oceans (Vance et al., 2009).

7. Conclusions:

The geochemistry of detrital sediment records holds valuable information on the weathering regime these sediments have undergone during their transit from sediment producing areas to their deposition in sedimentary basins. The chemical composition of these sediments is primarily controlled by sediment sorting effects that occur during transport and deposition. Nevertheless weathering signals can be extracted from the sediment chemical composition if sorting is properly taken into account by comparing sediment records to modern river systems.

The detrital record presented here shows that the degree of chemical weathering experienced by sediments exported by the Himalayan system, drained by the Ganga and Brahmaputra Rivers, has changed significantly since the LGM. An overall decrease in potassium and detrital calcite content along with an increase in sediment hydration all point towards a steady increase in the weathering degree of sediments over the last 21 kyrs, while the sediment provenance has remained unchanged. These changes in the weathering regime are attributed to the direct climatic forcing of chemical weathering in the floodplain, as increasing precipitation and temperatures after the deglaciation favored mineral weathering kinetics. Additional hydrological changes in response to increasing runoff and rising base level might also have impacted weathering through enhanced channel-floodplain interactions.

A first order estimation of changes in the weathering flux delivered to the oceans can be made using the detrital record and conservatively assuming a steady sediment flux. It

466 shows that weathering fluxes from the Himalayan system could have been reduced by 90 %
467 during the LGM. This supports previous evidence that current dissolved fluxes are likely
468 higher than average Quaternary estimates. These drastic changes in solute supply to the
469 oceans on glacial-interglacial time scales have to be accounted for to reconstruct global
470 oceanic biogeochemical cycles.
471
472 **Acknowledgments:**
473 This work was supported by French INSU program “Relief de la Terre” and ANR
474 Calimero. V.G. was supported by the U.S. National Science Fundation (Grant OCE-0851015,
475 OCE-0928582). We thank C. Guilmette for assistance in the lab. H. Schopka and two
476 anonymous reviewers are also thanked for their constructive comments that helped to improve
477 the manuscript. T.M. Harrison is acknowledged for the very efficient handling of the
478 manuscript.

References :

Bayon, G., Dennielou, B., Etoubleau, J., Ponzevera, E., Toucanne, S., Bermell, S., 2012. Intensifying Weathering and Land Use in Iron Age Central Africa. Science 335, 1219-1222. 10.1126/science.1215400

Blum, M.D., Tornqvist, T.E., 2000. Fluvial responses to climate and sea-level change: a review and look forward. Sedimentology 47, 2-48.

Bouchez, J., Gaillardet, J., France-Lanord, C., Maurice, L., Dutra-Maia, P., 2011a. Grain size control of river suspended sediment geochemistry: Clues from Amazon River depth profiles. Geochem. Geophys. Geosyst. 12, Q03008. 10.1029/2010gc003380

Bouchez, J., Lupker, M., Gaillardet, J., France-Lanord, C., Maurice, L., 2011b. How important is it to integrate riverine suspended sediment chemical composition with depth? Clues from Amazon River depth-profiles. Geochimica Et Cosmochimica Acta 75, 6955-6970. 10.1016/j.gca.2011.08.038

Carignan, J., Hild, P., Mevelle, G., Morel, J., Yeghicheyan, D., 2001. Routine analyses of trace elements in geological samples using flow injection and low pressure on-line liquid chromatography coupled to ICP-MS: A study of geochemical reference materials BR, DR-N, UB-N, AN-G and GH. Geostandards Newsletter-the Journal of Geostandards and Geoanalysis 25, 187-198.

Chabaux, F., Granet, M., Blaes, E., Dosseto, A., France-Lanord, C., Valier, V., 2009. Determination of source and transfer-time of river sediments in alluvial plain from U-series nuclides: Evidence from the Ganges River System. Geochimica Et Cosmochimica Acta 73, A203-A203.

Chabaux, F., Granet, M., France-Lanord, C., Stille, P., 2006. U-series in Himalayan rivers: Timescale of sedimentary transfer. Geochimica Et Cosmochimica Acta 70, A92-A92. 10.1016/j.gca.2006.06.097|ISSN 0016-7037

Clift, P.D., Giosan, L., Biusztajn, J., Campbell, I.H., Allen, C., Pringle, M., Tabrez, A.R., Danish, M., Rabbani, M.M., Alizai, A., Carter, A., Lueckge, A., 2008. Holocene erosion of the Lesser Himalaya triggered by intensified summer monsoon. Geology 36, 79-82. 10.1130/g24315a.1|issn 0091-7613

Cullen, J.L., 1981. Microfossil evidence for changing salinity patterns in the Bay of Bengal over the last 20000 years. Palaeogeography Palaeoclimatology Palaeoecology 35, 315-356.

Dosseto, A., Hesse, P.P., Maher, K., Fryirs, K., Turner, S., 2010. Climatic and vegetation control on sediment dynamics during the last glacial cycle. Geology 38, 395-398. 10.1130/g30708.1

Duplessy, J.C., 1982. Glacial to interglacial contrasts in the northern Indian Ocean, . Nature 295, 494-498.

Foster, G.L., Vance, D., 2006. Negligible glacial-interglacial variation in continental chemical weathering rates. Nature 444, 918-921. 10.1038/nature05365

France-Lanord, C., Derry, L., 1997. Organic carbon burial forcing of the carbon cycle from Himalayan erosion. Nature 390, 65-66.

France-Lanord, C., Derry, L., Michard, A., 1993. Evolution of the Himalaya since Miocene time: isotopic and sedimentologic evidence from the Bengal Fan, in: Treloar, P.J., Searle, M. (Eds.), Himalayan Tectonics. Geol. Soc. Lond., London, pp. 603-621.

Galy, A., France-Lanord, C., 2001. Higher erosion rates in the Himalaya: Geochemical constraints on riverine fluxes. Geology 29, 23-26.

Galy, A., France-Lanord, C., Derry, L.A., 1999. The strontium isotopic budget of Himalayan Rivers in Nepal and Bangladesh. Geochimica Et Cosmochimica Acta 63, 1905-1925.

Galy, V., François, L., France-Lanord, C., Faure, P., Kudrass, H., Palhol, F., Singh, S., 2008. C4 plants decline in the Himalayan basin since the Last Glacial Maximum. Quaternary Science Reviews 27, 1396-1409. doi:10.1016/j.quascirev.2008.04.005

Garzanti, E., Ando, S., France-Lanord, C., Censi, P., Vignola, P., Galy, V., Lupker, M., 2011. Mineralogical and chemical variability of fluvial sediments 2. Suspended-load silt (Ganga-Brahmaputra, Bangladesh). Earth and Planetary Science Letters 302, 107-120. 10.1016/j.epsl.2010.11.043

Garzanti, E., Ando, S., France-Lanord, C., Vezzoli, G., Censi, P., Galy, V., Najman, Y., 2010. Mineralogical and chemical variability of fluvial sediments 1. Bedload sand (Ganga-Brahmaputra, Bangladesh). Earth and Planetary Science Letters 299, 368-381. 10.1016/j.epsl.2010.09.017

Goodbred, S.L., 2003. Response of the Ganges dispersal system to climate change: a source-to-sink view since the last interstade. Sedimentary Geology 162, 83-104.

Granet, M., Chabaux, F., Stille, P., Dosseto, A., France-Lanord, C., Blaes, E., 2010. U-series disequilibria in suspended river sediments and implication for sediment transfer time in alluvial plains: The case of the Himalayan rivers. Geochimica Et Cosmochimica Acta 74, 2851-2865. 10.1016/j.gca.2010.02.016

Granet, M., Chabaux, F., Stille, P., France-Lanord, C., Pelt, E., 2007. Time-scales of sedimentary transfer and weathering processes from U-series nuclides: Clues from the Himalayan rivers. Earth and Planetary Science Letters 261, 389-406. 10.1016/j.epsl.2007.07.012|ISSN 0012-821X

Heroy, D., Kuehl, S., Goodbred, S., 2003. Mineralogy of the Ganges and Brahmaputra rivers: Implications for river switching and Late Quaternary climate change. Sedimentary Geology 155, 343-359.

Herzschuh, U., 2006. Palaeo-moisture evolution in monsoonal Central Asia during the last 50,000 years. Quaternary Science Reviews 25, 163-178.

Hoehndorf, A., Kudrass, H.R., France-Lanord, C., 2003. Transfer of the Sr isotopic signature of the Himalayas to the Bay of Bengal. Deep-Sea Research Part Ii-Topical Studies in Oceanography 50, 951-960. 10.1016/s0967-0645(02)00614-8|issn 0967-0645

Ittekkot, V., Kudrass, H.R., Quadfasel, D., Unger, D., 2003. The Bay of Bengal--An Introduction. Deep Sea Research Part II: Topical Studies in Oceanography 50, 853-854.

Jones, M.T., Pearce, C.R., Oelkers, E.H., 2012. An experimental study of the interaction of basaltic riverine particulate material and seawater. Geochimica Et Cosmochimica Acta 77, 108-120. 10.1016/j.gca.2011.10.044

Kudrass, H., Hofmann, A., Doose, H., Emeis, K., Erlenkeuser, H., 2001. Modulation and amplification of climatic changes in the Northern Hemisphere by the Indian summer monsoon during the past 80 k.y. Geology 29, 63-66.

Limmer, D.R., Bˆning, P., Giosan, L., Ponton, C., Kˆhler, C.M., Cooper, M.J., Tabrez, A.R., Clift, P.D., 2012. Geochemical record of Holocene to Recent sedimentation on the Western Indus continental shelf, Arabian Sea. Geochem. Geophys. Geosyst. 13, Q01008. 10.1029/2011gc003845

Lupker, M., Blard, P.-H., Lavé, J., France-Lanord, C., Leanni, L., Puchol, N., Charreau, J., Bourlès, D., 2012a. 10Be-derived Himalayan denudation rates and sediment budgets in the Ganga basin. Earth and Planetary Science Letters 333–334, 146-156. 10.1016/j.epsl.2012.04.020

Lupker, M., France-Lanord, C., Galy, V., Lave, J., Gaillardet, J., Gajurel, A.P., Guilmette, C., Rahman, M., Singh, S.K., Sinha, R., 2012b. Predominant floodplain over mountain weathering of Himalayan sediments (Ganga basin). Geochimica Et Cosmochimica Acta 84, 410-432. 10.1016/j.gca.2012.02.001

Lupker, M., France-Lanord, C., LavÈ, J., Bouchez, J., Galy, V., MÈtivier, F., Gaillardet, J., Lartiges, B., Mugnier, J.-L., 2011. A Rouse-based method to integrate the chemical composition of river sediments: Application to the Ganga basin. J. Geophys. Res. 116, F04012. 10.1029/2010jf001947

Michalopoulos, P., Aller, R.C., 1995. Rapid Clay Mineral Formation in Amazon Delta Sediments: Reverse Weathering and Oceanic Elemental Cycles. Science 270, 614.

Michalopoulos, P., Aller, R.C., 2004. Early diagenesis of biogenic silica in the Amazon delta: alteration, authigenic clay formation, and storage. Geochimica Et Cosmochimica Acta 68, 1061-1085. 10.1016/j.gca.2003.07.018

Michels, K.H., Kudrass, H.R., H¸bscher, C., Suckow, A., Wiedicke, M., 1998. The submarine delta of the Ganges-Brahmaputra: cyclone-dominated sedimentation patterns. Marine Geology 149, 133-154.

Pierson-Wickmann, A.-C., Reisberg, L., France-Lanord, C., Kudrass, H., 2001. Os-Sr-Nd results from sediments in the Bay of Bengal: Implications for sediment transport and the marine Os record. Paleoceanography 16, 435-444.

Rahaman, W., Singh, S.K., Sinha, R., Tandon, S.K., 2009. Climate control on erosion distribution over the Himalaya during the past ~100 ka. Geology 37, 559-562. 10.1130/g25425a.1

Rahaman, W., Singh, S.K., Sinha, R., Tandon, S.K., 2010. Climate control on erosion distribution over the Himalaya during the past similar to 100 ka: REPLY. Geology 38, E217-E217. 10.1130/g31119y.1

Ramankutty, N., Foley, J.A., 1999. Estimating historical changes in global land cover: Croplands from 1700 to 1992. Global Biogeochem. Cycles 13, 997-1027. 10.1029/1999gb900046

Raymo, M., Ruddiman, W., Froelich, P., 1988. Influence of late Cenozoic mountain building on ocean geochemical cycles. Geology 16, 649.

Reimer, P.J., Baillie, M.G.L., Bard, E., Bayliss, A., Beck, J.W., Blackwell, P.G., Ramsey, C.B., Buck, C.E., Burr, G.S., Edwards, R.L., Friedrich, M., Grootes, P.M., Guilderson, T.P., Hajdas, I., Heaton, T.J., Hogg, A.G., Hughen, K.A., Kaiser, K.F., Kromer, B., McCormac, F.G., Manning, S.W., Reimer, R.W., Richards, D.A., Southon, J.R., Talamo, S., Turney, C.S.M., van der Plicht, J., Weyhenmeye, C.E., 2009. Intcal09 and Marine09 Radiocarbon Age Calibration Curves, 0-50,000 Years Cal Bp. Radiocarbon 51, 1111-1150.

RSP, 1996. River Survey Project, Flood Action Plan (FAP) final report. Delft Hydraulics and DHI.

Sanyal, P., Bhattacharya, S.K., Prasad, M., 2005. Chemical diagenesis of Siwalik sandstone: Isotopic and mineralogical proxies from Surai Khola section, Nepal. Sedimentary Geology 180, 57-74.

Sharma, S., Joachimski, M., Sharma, M., Tobschall, H.J., Singh, I.B., Sharma, C., Chauhan, M.S., Morgenroth, G., 2004. Lateglacial and Holocene environmental changes in Ganga plain, Northern India. Quaternary Science Reviews 23, 145-159.

Singh, S., France-Lanord, C., 2002a. Tracing the distribution of erosion in the Brahmaputra watershed from isotopic compositions of stream sediments. Earth and Planetary Science Letters 252, 645-662.

Singh, S.K., France-Lanord, C., 2002b. Erosion distribution in the Eastern Himalaya traced by Sr-Nd isotopic compositions of river sediments. Geochimica Et Cosmochimica Acta 66, A720-A720.

Singh, S.K., Rai, S.K., Krishnaswami, S., 2008. Sr and Nd isotopes in river sediments from the Ganga Basin: Sediment provenance and spatial variability in physical erosion. J. Geophys. Res. 113, F03006. 10.1029/2007jf000909

627 **Singh, S.K., Sarin, M.M., France-Lanord, C., 2005. Chemical erosion in the eastern**
628 **Himalaya: Major ion composition of the Brahmaputra and delta C-13 of dissolved**
629 **inorganic carbon. Geochimica Et Cosmochimica Acta 69, 3573-3588.**
630 **10.1016/j.gca.2005.02.033|ISSN 0016-7037**
631 **Srivastava, P., Shukla, U.K., 2010. Climate control on erosion distribution over the**
632 **Himalaya during past similar to 100 ka: COMMENT. Geology 38, E216-E216.**
633 **10.1130/g30838c.1**
634 **Vance, D., Teagle, D.A.H., Foster, G.L., 2009. Variable Quaternary chemical weathering**
635 **fluxes and imbalances in marine geochemical budgets. Nature 458, 493-496.**
636 **10.1038/nature07828**
637 **Walker, J., Hays, P., Kasting, J., 1981. A negative feedback mechanism for the long-**
638 **term stabilization of the Earth's surface temperature. Journal of Geophysical Research**
639 **86, 9776-9782.**
640 **Wallmann, K., Aloisi, G., Haeckel, M., Tishchenko, P., Pavlova, G., Greinert, J.,**
641 **Kutterolf, S., Eisenhauer, A., 2008. Silicate weathering in anoxic marine sediments.**
642 **Geochimica Et Cosmochimica Acta 72, 2895-2918.**
643 **Weber, M.E., Wiedicke, M.H., Kudrass, H.R., Hübscher, C., Erlenkeuser, H., 1997.**
644 **Active growth of the bengal Fan during sea-level rise and highstand. Geology 25, 315-**
645 **318.**
646 **West, A.J., Bickle, M.J., Collins, R., Brasington, J., 2002. Small-catchment perspective**
647 **on Himalayan weathering fluxes. Geology 30, 355-358. 10.1130/0091-**
648 **7613(2002)030<0355:scpohw>2.0.co;2**
649 **White, A.F., Blum, A.E., 1995. Effects of climate on chemical weathering in watersheds.**
650 **Geochimica et Cosmochimica Acta 59.**
651 **Willenbring, J.K., von Blanckenburg, F., 2011. Long-term stability of global erosion**
652 **rates and weathering during late-Cenozoic cooling. Nature 465, 211-214.**
653 **10.1038/nature09044**
654
655

656

Figures:

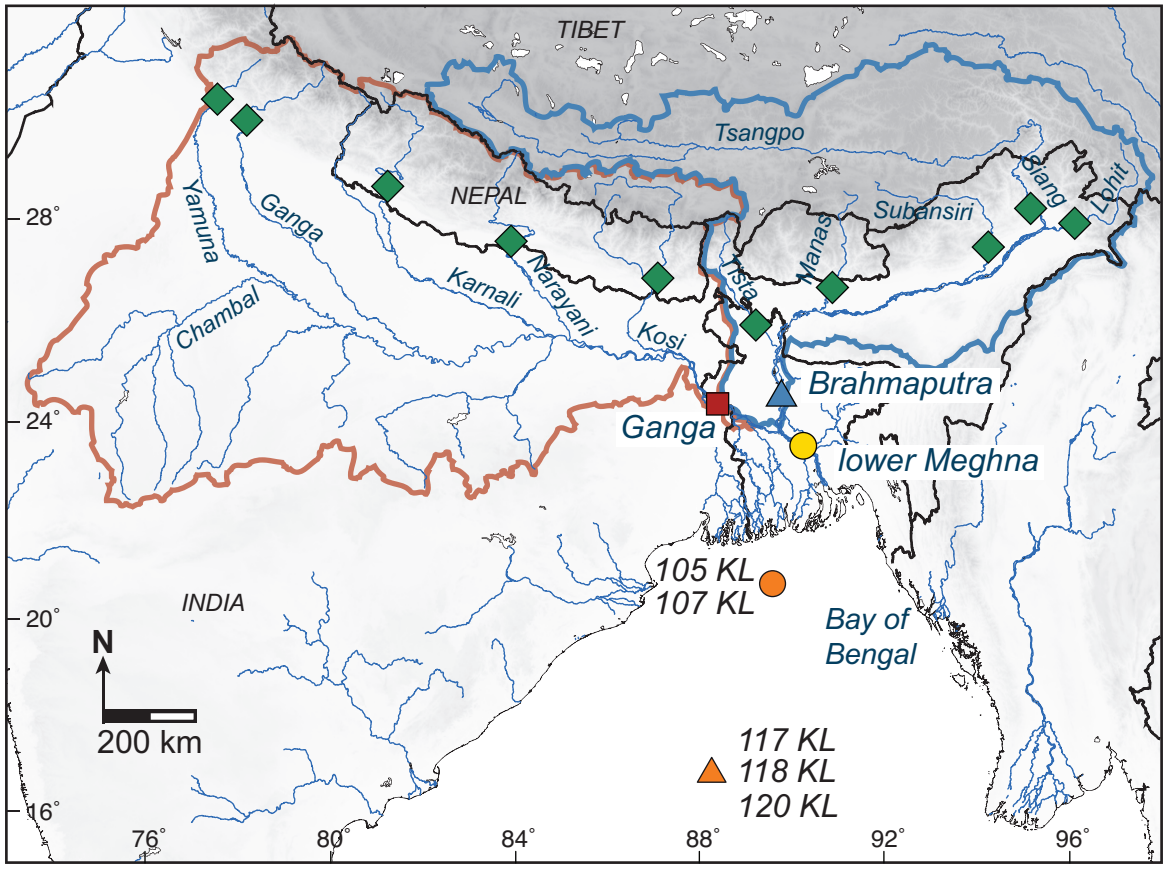

Figure 1: Geographical setting of the Himalayan system. Modern river sediments were sampled in the Ganga & Brahmaputra basin at the Himalayan front (green diamonds), at the outlet of the Ganga basin (red square) and the Brahmaputra basin (blue triangle) and finally after their confluence in the lower Meghna (yellow circle). These sediments were compared to the sediment record of the Bay of Bengal that represents a composite record from proximal shelf sediments (105KL and 107KL) and from the middle fan channel levees (117KL, 118KL and 120KL).

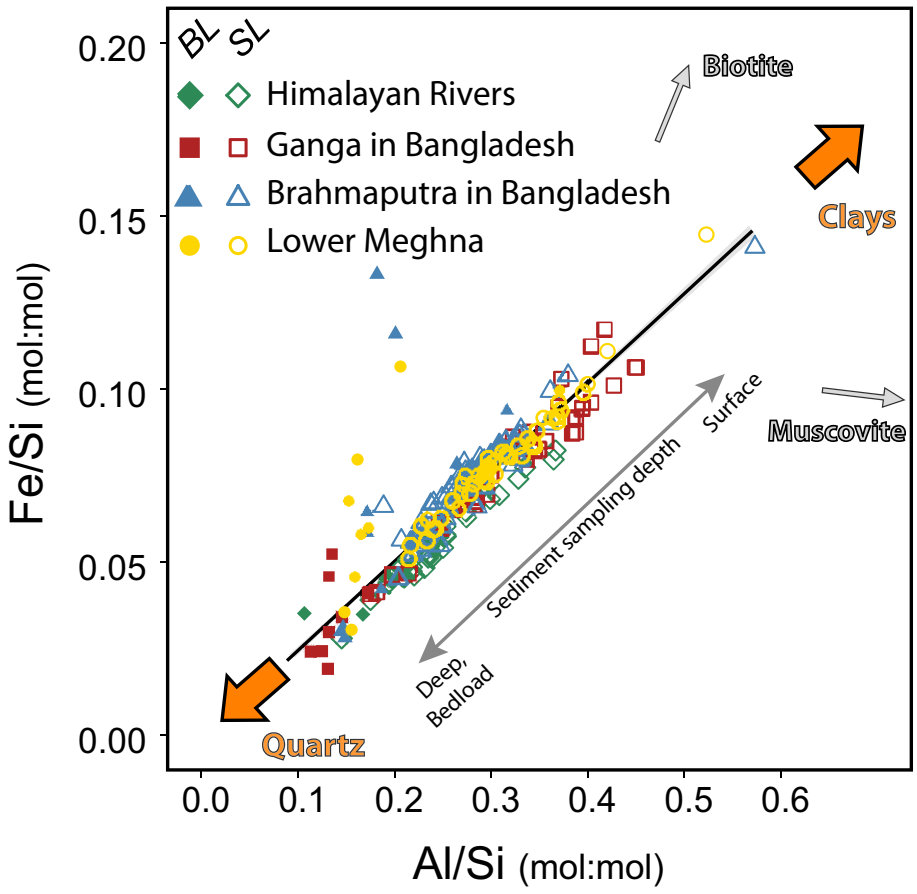

667

668 **Figure 2:** Hydraulic sorting effect on the Si-Al-Fe chemical composition of sediments.
669 Suspended sediments are the result of the mixing between a low Al/Si and Fe/Si
670 quartz-rich coarse-grained end-member and a high Al/Si and Fe/Si surface end-
671 member relatively enriched in phylosilicates.

672

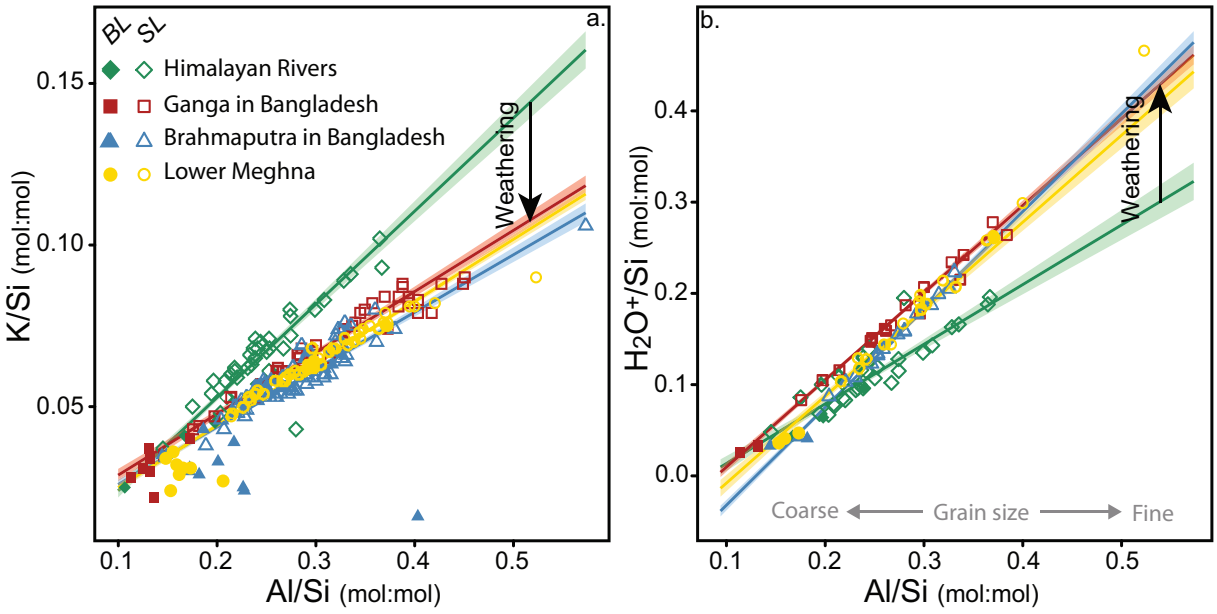

673

674 **Figure 3:** Evolution of K/Si (a) and H_2O^+/Si (b) in the modern Himalayan system for river
675 suspended load (SL) and bedload or bar sediments (BL). The transfer of sediments
676 from the Himalayan front Rivers (green) to the outlet of the Ganga (red) and
677 Brahmaputra (blue), as well as their confluence the lower-Meghna (yellow) results in
678 a loss of K and an increase in H_2O^+ as weathering proceeds. Envelopes represent 0.95
679 confidence level on the linear regression.

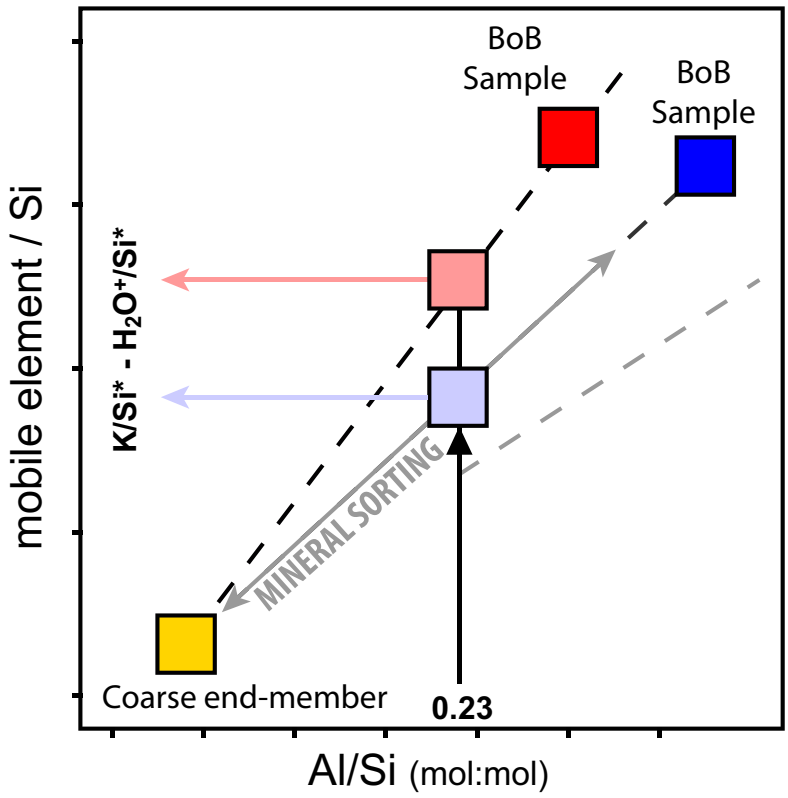

680

681 **Figure 4:** Normalization of the chemical composition of sediments in of the Bay of Bengal
682 record for hydraulic sorting effects. The K/Si and H_2O^+/Si ratios of the sample are
683 normalized to a common Al/Si ratio of 0.23 assuming that the sediment sorting line
684 passes through a unique coarse-grained end-member with a composition close to river
685 bedloads (given in the supplementary information, Table S1).

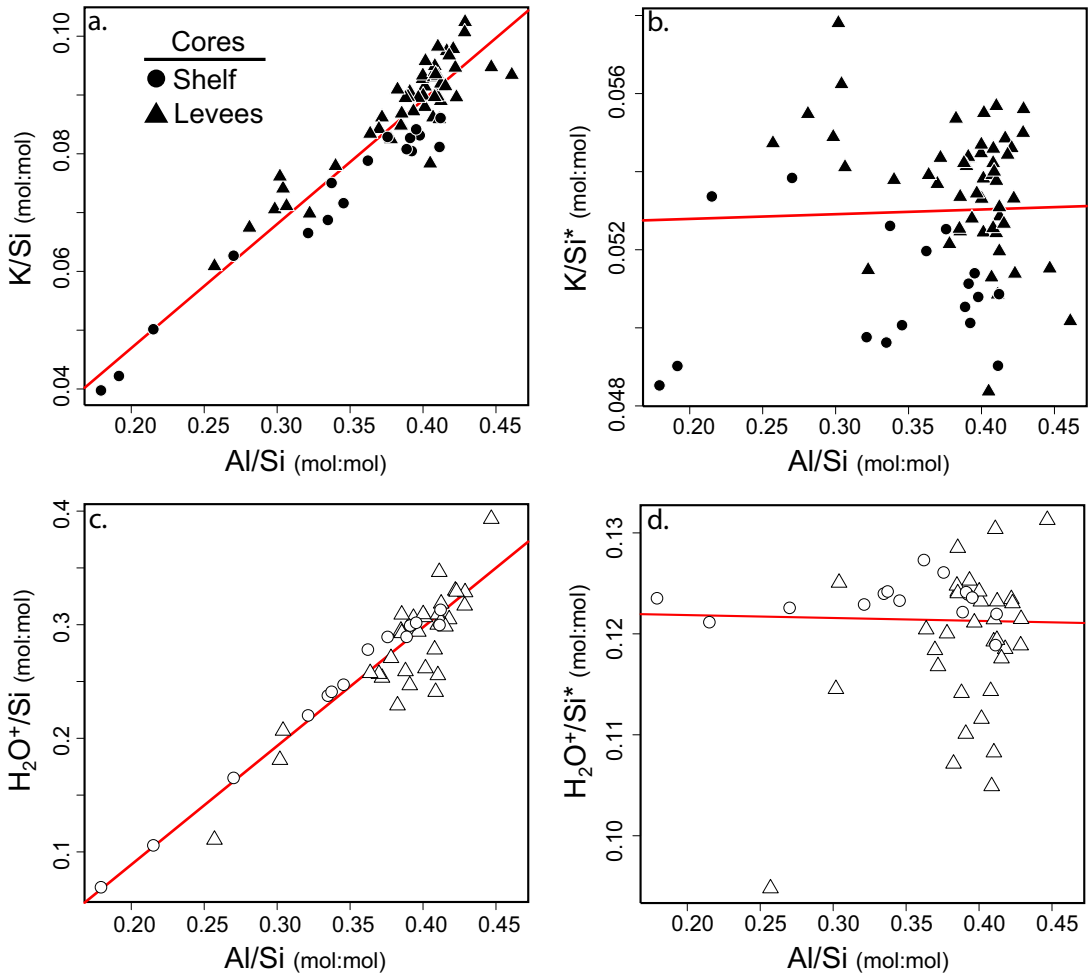

686

687 **Figure 5:** K/Si and H_2O^+/Si in Bay of Bengal core sediments are strongly correlated to Al/Si,
688 which is a proxy for grain size (Bouchez et al., 2011a; Lupker et al., 2011). Correction
689 for hydraulic mineral sorting yields unbiased weathering indicators (K/Si* and
690 H_2O^+/Si*).

691

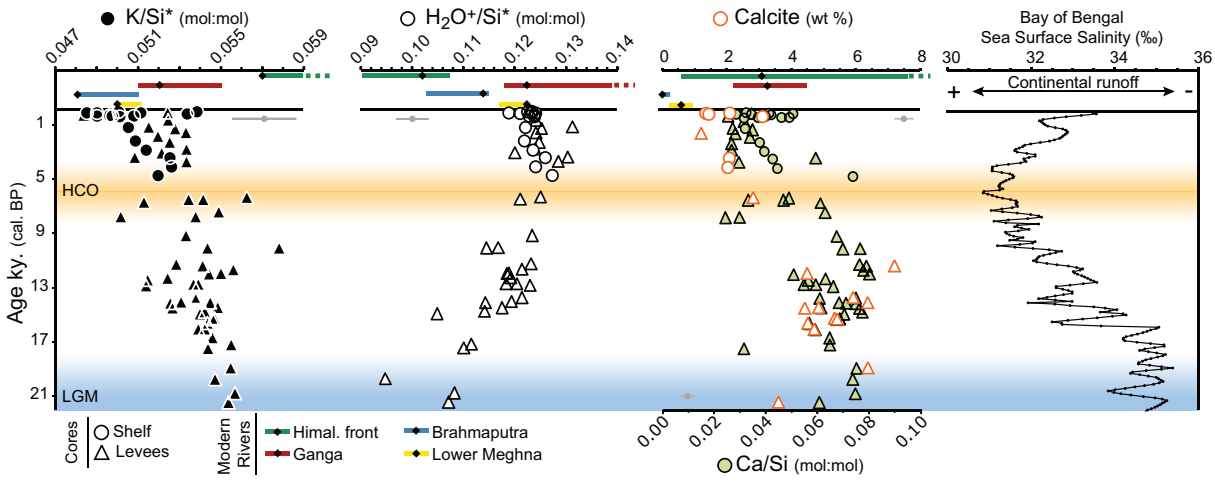

Figure 6: Evolution of K/Si*, H_2O^+/Si*, Ca/Si and calcite content of sediments in the composite Bay of Bengal record since the last ca. 21 kyr. The composition of river sediments from the modern Himalayan system (average and 1st - 3rd quartile range) is also plotted for comparison with the sediment record. The Bay of Bengal sea surface salinity (Kudrass et al., 2001) is shown as a proxy for the Ganga & Brahmaputra continental runoff. The average, 1σ uncertainty on the elemental ratios is indicated by light grey horizontal error bars.

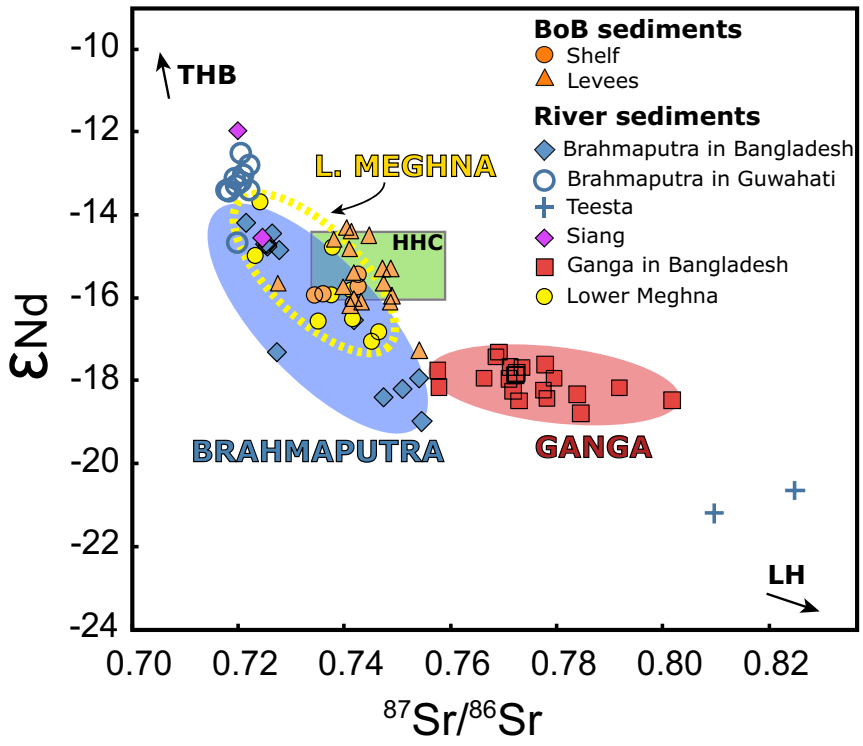

701

702 **Figure 7:** Sr and Nd isotopic composition of the sediments from the Bay of Bengal.
703 The modern river sediments of the Ganga in Bangladesh, the Brahmaputra in Bangladesh
704 (along with samples from the Siang, the Brahmaputra in Guwahati and the Teesta, Rivers
705 from Singh and France-Lanord, 2002) and the lower Meghna are represented for comparison.
706 The Sr and Nd isotopic data set of the Brahmaputra in Bangladesh has partly been acquired in
707 order to test sediment source effects in the Brahmaputra basin by selecting samples that
708 covered a large span of chemical compositions. This sample choice may have introduced a
709 bias towards samples that recorded a large input from the Teesta upstream right-bank
710 tributary. We therefore suspect the average Sr and Nd isotopic composition of the
711 Brahmaputra to be closer to the Brahmaputra in Guwahati and the Siang than our dataset
712 suggests (see supplementary information). The isotopic composition of the Lesser Himalaya
713 (LH), Higher Himalaya Cristalines (HHC) and Trans Himalayan Batholith (THB) are from
714 Galy and France-Lanord (2001) and references therein.

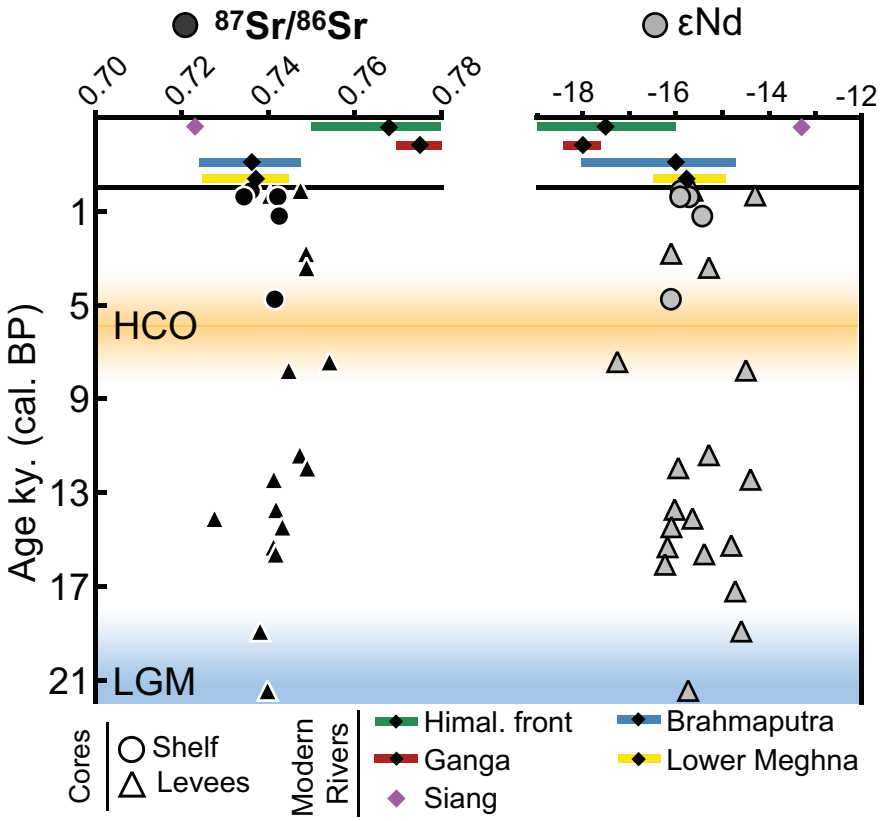

715

716 **Figure 8:** Sr and Nd isotopic composition of the silicate fraction of Bay of Bengal sediments
717 (Pierson-Wickmann et al., 1998; Galy et al., 2008 and this study) along with the
718 modern river sediments composition of the Himalayan front, the Ganga, the
719 Brahmaputra and the lower Meghna (average and 1st - 3rd quartile range). The isotopic
720 composition of sediments from the modern Siang River (Singh and France-Lanord,
721 2002b) is also plotted. The Siang delivers ca. 50 % of the sediment load of the
722 Brahmaputra (Singh and France-Lanord, 2002b), contributing disproportionally to the
723 final isotopic signature of the modern Brahmaputra.

724

Tables

		LGM	Modern
Sediment flux (t/yr)		1.10^9	1.10^9
Himalayan front	$\overline{K/Si^*}$	0.0574 (±0.0025)	0.0574 (±0.0025)
	$\overline{H_2O^+/Si^*}$	0.1009 (±0.0068)	0.1009 (±0.0068)
Bay of Bengal	$\overline{K/Si^*}$	0.0553 (±0.0005)	0.0510 (±0.0017)
	$\overline{H_2O^+/Si^*}$	0.1034 (±0.0075)	0.1236 (±0.0026)
	$R\phi_K$	67 (±28) %	
	$R\phi_{H2O+}$	89 (±36) %	

Table 1: Relative changes in the weathering flux delivered to the Bay of Bengal as dissolved load from the LGM to present ($R\varphi_K$ and $R\varphi_{H2O+}$) assuming a constant sediment flux over the period. The weathering flux was estimated using eq. 3 for K and H_2O^+ from the Himalayan front and Bay of Bengal end-members reported in the table.

731 **Supplementary information and data:**

732

733 **S1 – Chemical weathering proxies and data:**

734 The coarse grained end-members used to normalize the chemical composition of the
735 Bay of Bengal sediments are reported in Table S1. This coarse-grained mixing end-member is
736 determined as the intersection between the linear regression through the composition of
737 Himalayan front sediments and the composition of sediments in Bangladesh (Ganga,
738 Brahmaputra and lower Meghna) for K/Si and H_2O^+/Si. For Fe/Si (used in section S2), the
739 common coarse-grained end-member composition is defined by the intersection between the
740 regressions through Himalayan front sediments and southern and eastern tributary sediments
741 (Chambal, Lohit and Dibang) as sediments from these rivers show a very contrasted Fe/Si
742 composition. This method was preferred over averaging all available bedloads as placer
743 effects tend to introduce a very high variability in the chemical composition of the bedloads,
744 which is not found in suspended load samples and therefore does not accurately describe the
745 sediments that are mixed in the water column.

746 A summary of the composition of modern river sediments is reported in Table S2 and
747 the composition of Bay of Bengal sediments in Table S3. The full, detailed data set of modern
748 sediments and Bay of Bengal sediments is provided as electronic appendix.

749

750 **S2 - Sediment provenance:**

751 *Sr & Nd signature of Brahmaputra sediments:*

752

753 It should be noted that the Sr and Nd isotopic data set of the Brahmaputra in
754 Bangladesh has partly been acquired in order to test sediment source effects in the
755 Brahmaputra basin by selecting samples that covered the largest span of chemical

compositions. This sample choice introduces a bias towards samples impacted by the influx from an upstream right-bank tributary, the Teesta, which has high εNd and low $^{87}Sr/^{86}Sr$ values (Figure 7). We therefore suspect the average Sr and Nd isotopic composition of the Brahmaputra to be closer to that of the Brahmaputra in Guwahati (higher for Nd and lower for Sr) than our whole dataset suggests.

The Sr and Nd isotopic composition of Brahmaputra sediments sampled at Guwahati, upstream of the confluence with the Teesta show a homogeneous composition of 0.7201 ± 0.0014 $^{87}Sr/^{86}Sr$ and -13.3 ± 0.7 εNd (Figure 7, Singh and France-Lanord, 2002). These sediments are mainly derived from the erosion of the Namche Barwa zone by the Siang River that accounts for ca. 50 % of the Brahmaputra sediment load (Singh and France-Lanord, 2002). The Teesta River has a contrasted isotopic composition due to the dominant exposure of Lesser Himalayan rocks in the basin (Figure 7, Singh and France-Lanord, 2002) and its confluence with the Brahmaputra mainstream is only ca. 120 km upstream of our sampling station in Bangladesh. These considerations may also explain why the contribution of Brahmaputra sediments to the lower Meghna is overestimated based on a simple Sr and Nd isotopic budget of the Ganga, Brahmaputra and lower Meghna.

Increase in Southern or Eastern tributaries and Siwalik contribution since the LGM:

An increase in Siwalik derived sediments would generate a more weathered signature of the Ganga & Brahmaputra sediment load. Because Siwalik are Neogene floodplain deposits produced by Himalayan erosion and uplifted by the southern propagation of the deformation front, Siwalik sediments have a more weathered silicate signature but similar Sr and Nd isotopic compositions than trans-Himalayan river sediments (Lupker et al., 2012). However, the high carbonate content with lower $\delta^{13}C$ compositions of Siwalik rocks and

781 sediments (e.g. Sanyal et al., 2005; Lupker et al., 2012) is not compatible with the
782 concomitant decrease of both carbonate content and $\delta^{13}C$ found in the Bay of Bengal
783 sediments (Figure S1).

784 Further changes in erosion patterns involving cratonic tributaries are also unlikely.
785 The Chambal River in the Ganga basin and the Eastern tributaries of the Brahmaputra basin
786 (Lohit and Dibang) have distinctively higher Fe/Si* ratios and unradiogenic Sr and Nd (Singh
787 et al., 2002; Singh et al., 2008; Lupker et al., 2012) signature that are not identified in our
788 record (Figure S1).

789

790 **S3 – Uncertainties and sensitivity of the weathering budget to the average Al/Si ratio:**

791

792 The analytical uncertainty from the major element and H_2O^+ measurements is 2% on
793 the Al/Si and Fe/Si ratios, 3% on the K/Si and H_2O^+/Si ratios (Carignan et al., 2001). The
794 uncertainty on the definition of the coarse grained end-member (Table S1) has only a minor
795 effect on the normalized K/Si* and H_2O^+/Si* ratios. For an average Bay of Bengal sediment
796 sample with an Al/Si ratio of 0.38, the total uncertainty propagated from the analytical and
797 normalization uncertainty is ca. 3% for the K/Si*, H_2O^+/Si* and Fe/Si* ratios on a 1σ
798 confidence level.

799 The sensitivity of the weathering budget to the average Al/si ratio of the sediments is
800 assessed by comparing Rφ determined for an Al/Si of 0.23 to Rφ obtained using an Al/Si of
801 0.21 and 0.25 (Table S4). This corresponds to ca. 10% of uncertainty on Al/Si and is higher
802 than the ca. 5% uncertainty estimated by Lupker et al. (2011) for the average Al/Si
803 composition of sediments of the Ganga River but it takes into account the fact that in this case
804 the average Al/Si ratio of Brahmaputra sediments has not been determined directly. Table S4
805 shows that for the sensitivity of the weathering budget to the average Al/Si is limited for a

806 reasonable range of Al/Si ratios.

Supplementary information figures:

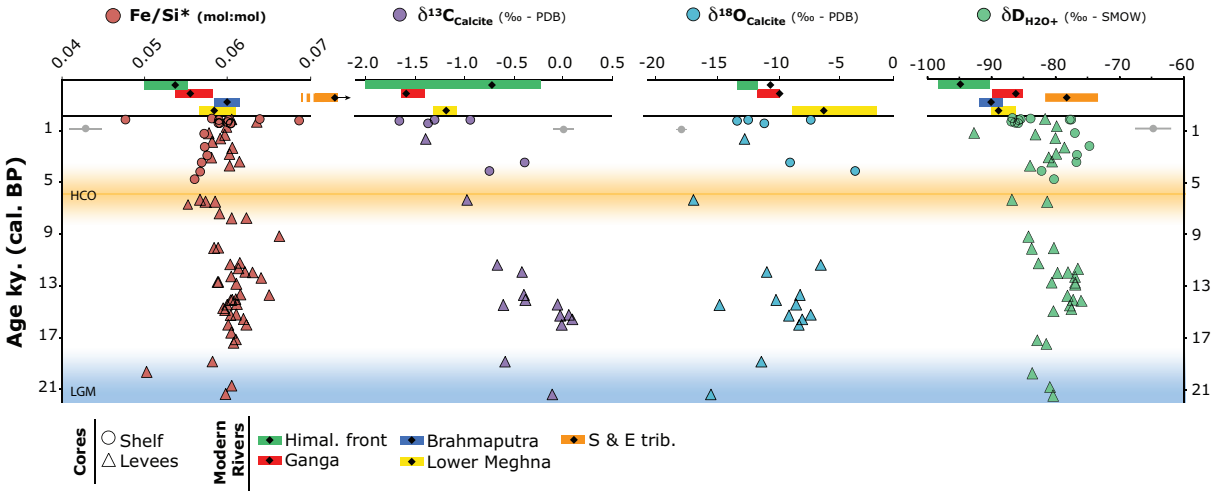

Figure S1: Fe/Si*, $\delta^{13}C_{PDB}$, $\delta^{18}O_{PDB}$ of calcite and δD_{H2O+} in Bay of Bengal core samples and modern rivers (average and 1st - 3rd quartile range).

Supplementary information tables:

K/Si*	K/Si	0.029 ± 0.001
	Al/Si	0.117 ± 0.005
H_2O^+/Si*	H_2O^+/Si	0.060 ± 0.002
	Al/Si	0.171 ± 0.003
Fe/Si*	Fe/Si	0.020 ± 0.003
	Al/Si	0.087 ± 0.004

Table S1: Coarse-load mixing end-members used for the correction of hydraulic sorting effects on the chemical composition of sediments.

817 **Table S2:**

		Ganga Himalayan Front	Brahmaputra Himalayan Front	Himalayan Front Rivers[a]	Ganga	Brahmaputra	L. Meghna	S. and E. tributaries
K/Si*	**Mean[b]**	0.063	0.054	0.057	0.052	0.048	0.050	0.036
	sd[b]	0.001	0.004	0.002	0.001	0.001	0.001	0.007
	1st Q	0.061	0.051	0.057	0.051	0.048	0.050	0.029
	Median	0.062	0.055	0.061	0.054	0.049	0.050	0.039
	3rd Q	0.065	0.057	0.065	0.055	0.051	0.051	0.060
	n	39	14	53	68	106	60	6
H_2O^+/ Si*	**Mean[b]**	0.099	0.102	0.101	0.122	0.114	0.122	0.065
	sd[b]	0.003	0.011	0.007	0.005	0.003	0.002	0.004
	1st Q	0.093	0.082	0.090	0.118	0.103	0.117	0.083
	Median	0.099	0.089	0.098	0.127	0.112	0.119	0.118
	3rd Q	0.109	0.104	0.107	0.142	0.115	0.122	0.159
	n	32	12	44	26	26	21	4
Fe/Si*	**Mean[b]**	0.052	0.055	0.054	0.056	0.060	0.059	0.082
	sd[b]	0.001	0.004	0.003	0.001	0.007	0.002	0.012
	1st Q	0.050	0.052	0.050	0.054	0.059	0.057	0.077
	Median	0.052	0.056	0.053	0.055	0.061	0.058	0.078
	3rd Q	0.054	0.061	0.055	0.058	0.062	0.061	0.096
	n	39	14	53	68	106	60	6
Calcite (wt%)	**Mean**	6.4	0.9	3.1	3.4	-	0.6	5.1
	sd	6.0	1.1	2.5	1.3	-	0.8	3.1
	1st Q	0.8	0.0	0.6	2.2	-	0.2	2.8
	Median	4.0	0.1	3.1	3.9	-	0.2	4.9
	3rd Q	12.1	2.0	11.1	4.5	-	0.8	6.8
	n	31	5	36	30	-	6	5
$\delta^{13}C_{Calcite}$ (‰ - PDB)	**Mean**	-1.3	-0.3	-0.7	-1.6	-	-1.2	-0.7
	sd	1.2	0.8	0.7	0.4	-	0.1	1.6
	1st Q	-2.1	-0.6	-2.0	-1.6	-	-1.3	-1.8
	Median	-1.2	0.0	-1.2	-1.5	-	-1.2	-1.5
	3rd Q	-0.5	0.1	-0.3	-1.4	-	-1.1	0.2
	n	29	3	32	27	-	3	5
$\delta^{18}O_{Calcite}$ (‰ - PDB)	**Mean**	-12.3	-9.4	-10.6	-10.0	-	-6.2	-6.8
	sd	1.4	3.8	2.3	2.6	-	6.2	3.7
	1st Q	-13.2	-11.6	-13.2	-11.6	-	-8.4	-9.8
	Median	-12.5	-11.4	-12.4	-10.4	-	-3.5	-4.4
	3rd Q	-12.2	-8.2	-11.7	-10.0	-	-2.6	-4.4
	n	29	3	32	27	-	3	5
Ca/Si	**Mean**	0.115	0.027	0.062	0.058	0.042	0.043	0.115
	sd	0.075	0.021	0.002	0.017	0.018	0.015	0.038
	1st Q	0.040	0.017	0.028	0.042	0.036	0.032	0.098
	Median	0.104	0.018	0.064	0.063	0.040	0.039	0.108
	3rd Q	0.170	0.022	0.153	0.072	0.042	0.050	0.137
	n	39	14	53	68	106	60	6
$^{87}Sr/^{86}Sr$	**Mean**	0.7713	0.7660	0.76813	0.77491	0.73562	0.73694	0.70705
	sd	0.0101	0.0439	0.02665	0.01009	0.01271	0.00833	-
	1st Q	0.7647	0.7329	0.74925	0.77111	0.72560	0.72547	-
	Median	0.7726	0.7600	0.76440	0.77252	0.72779	0.73790	-
	3rd Q	0.7769	0.7870	0.77921	0.77825	0.74756	0.74157	-
	n	8	11	19	21	13	9	2
εNd	**Mean**	-18.9	-16.6	-17.5	-18.0	-16.2	-15.8	-9.7
	sd	0.9	3.5	2.3	0.4	1.5	1.1	-
	1st Q	-19.3	-18.9	-19.3	-18.3	-18.0	-16.5	-
	Median	-18.8	-16.0	-18.2	-18.0	-16.0	-15.9	-
	3rd Q	-18.3	-14.4	-16.0	-17.8	-14.7	-15.0	-
	n	10	11	21	22	13	9	2

818

Table S2: Averaged chemical composition of samples from the Himalayan system. The compositions are given separately for samples from the Ganga Himalayan front, the Brahmaputra Himalayan front, the average Himalayan front, the Ganga in Bangladesh, the Brahmaputra in Bangladesh, the lower Meghna (confluence of the Ganga & Brahmaputra) and southern and eastern tributaries. [a]The Himalayan front is reconstructed assuming that 60 % of the total sediment flux is generated by front rivers in the Brahmaputra basin and 40 % by the front rivers in the Ganga basin. [b]For element ratios affected by sediment sorting, the average and standard deviation of each end-member is constrained by evaluating the linear regression through the entire data set of each reach under consideration along with the coarse-grained end-member at Al/Si=0.23. The 1st and 3rd quartile, median and number of samples are also reported for all reaches. Detail on the chemical composition of samples used can be found in the electronic appendix.

833 **Table S3:**

Core	Depth	Age	Al/Si	K/Si*	H2O/Si*	Ca/Si	Fe/Si*		Calcite			^{87}Sr	eNd
	cm	yr BP	mol	mol	mol	mol	mol	dD	wt%	d^{13}C	d^{18}O	Sil	Sil
105	77-86	47	0.346	0.050	0.123	0.032	0.058	-87					
105	129	74	0.270	0.054	0.123	0.041	0.064	-84					
118	7-17	98	0.401	0.052	0.123	0.032	0.060	-82				0.74740	-15.7
105	241	138	0.179	0.049	0.124	0.051	0.048	-85	2.1	-1.3	-12.5	0.73600	-15.9
107	50-60	147	0.391	0.051	0.124	0.034	0.059	-78	1.4	-0.9	-7.5		
105	279-285	161	0.411	0.049	0.119	0.028	0.060	-78					
107	80	213	0.215	0.053	0.121	0.042	0.069	-86	1.4	-1.6	-13.4		
118	29	313	0.405	0.048		0.034	0.063					0.74040	-14.3
105	564-572	325	0.335	0.050	0.124	0.040	0.060	-87					
105	664-670	382	0.398	0.051		0.037	0.060					0.74218	-15.7
105	678-685	390	0.321	0.050	0.123	0.046	0.059	-86					
105	686-690	394	0.192	0.049		0.049	0.059		3.1	-1.3	-11.2	0.73437	-15.9
105	758-765	436	0.392	0.050	0.124	0.032	0.060	-86					
118	70-80	681	0.385	0.052	0.124	0.025	0.060	-80					
120	53	1184	0.447	0.052	0.131	0.024	0.058	-93					
107	145-155	1214	0.389	0.051	0.122	0.032	0.057	-77				0.74255	-15.4
118	134-145	1302	0.393	0.053	0.125	0.032	0.060	-83					
118	165-175	1603	0.400	0.053	0.124	0.035	0.059	-80	1.2	-1.4	-12.8		
120	83	1854	0.412	0.052		0.027	0.058						
107	210-220	2212	0.412	0.051	0.122	0.038	0.057	-75					
118	220-230	2317	0.385	0.053	0.125	0.028	0.060	-79					
118	265-275	2799	0.385	0.053	0.124	0.027	0.060	-80				0.74872	-16.1
107	255-265	2904	0.395	0.051	0.124	0.040	0.057	-77					
120	138	3083	0.378	0.052	0.120	0.034	0.058	-81					
120	147-157	3396	0.411	0.051	0.130	0.103	0.061	-80				0.74879	-15.3
107	291-301	3457	0.376	0.053	0.126	0.043	0.057	-77	2.1	-0.4	-9.1		
118	340-350	3717	0.385	0.053	0.129	0.027	0.060	-84					
107	335-345	4133	0.337	0.053	0.124	0.044	0.057	-82	2.0	-0.7	-3.9		
107	376-385	4748	0.362	0.052	0.127	0.074	0.056	-80				0.74153	-16.1
120	284	6345	0.304	0.056	0.125	0.059	0.057	-87	2.8	-1.0	-16.9		
118	565-575	6496	0.397	0.053	0.121	0.030	0.058	-81					
118	575	6496	0.390	0.054		0.047	0.057						
118	656	6719	0.407	0.051		0.033	0.055						
118	920	7418	0.298	0.055		0.061	0.059					0.75414	-17.3
120	348	7775	0.461	0.050		0.049	0.062					0.74467	-14.5
118	1144	7787	0.340	0.054		0.063	0.060						
120	411	9182	0.422	0.053	0.123	0.030	0.066	-84					
117	242-257	10070	0.372	0.054	0.117	0.082	0.059	-80					
120	452	10098	0.302	0.058	0.115	0.067	0.058	-84					
120	555	11255	0.412	0.053	0.123	0.070	0.061	-83					
120	579	11376	0.306	0.054		0.076	0.060		7.2	-0.7	-6.6	0.74723	-15.3
120	632-642	11668	0.429	0.056	0.121	0.079	0.061	-76					
120	691-701	11940	0.429	0.055	0.119	0.078	0.062	-78	4.5	-0.4	-11.0	0.74899	-16.0
120	701	11991	0.418	0.054	0.119	0.080	0.063	-80					
120	762	12298	0.410	0.052	0.119	0.051	0.060	-77					
120	787	12424	0.322	0.051		0.063	0.064					0.74129	-14.4
120	848	12731	0.370	0.054	0.118	0.056	0.059	-77					
120	845-855	12736	0.364	0.054	0.120	0.059	0.059	-81					
120	863	12865	0.423	0.051	0.123	0.055	0.061	-77					
117	722-725	13712	0.401	0.054		0.077	0.061		5.9	-0.4	-8.3	0.74180	-16.0
120	929-939	13744	0.410	0.054	0.121	0.066	0.065	-78					
120	959	14053	0.412	0.053	0.119	0.061	0.061	-77					
117	772-774	14096	0.400	0.054		0.075	0.060		6.4	-0.4	-10.2	0.72754	-15.7

120	965	14127	**0.408**	0.053	0.114	0.068	0.060	-76					
117	819-822	14457	**0.416**	0.055		0.071	0.061		4.9	0.0	-8.6	**0.74324**	**-16.1**
120	990-1000	14498	**0.415**	0.053	0.118	0.075	0.060	-78	4.4	-0.6	-14.8		
120	1016	14758	**0.388**	0.054	0.114	0.076	0.059	-77					
120	1030	14931	**0.409**	0.054	0.105	0.077	0.060	-80					
117	922-925	15249	**0.400**	0.055		0.061	0.061		5.3	0.1	-7.4	**0.74100**	**-14.8**
117	930-932	15310	**0.421**	0.055		0.069	0.060		5.4	0.0	-9.2	**0.74115**	**-16.2**
117	970-972	15610	**0.391**	0.054		0.067	0.062		4.5	0.1	-8.1	**0.74172**	**-15.4**
117	1025-1029	16048	**0.408**	0.054		0.057	0.060		4.7	0.0	-8.4		**-16.2**
117	1027-1029	16056	**0.407**	0.054		0.059	0.062						
117	1106-1109	16663	**0.408**	0.055		0.059	0.060						
117	1175	17185	**0.402**	0.056	0.112	0.065	0.061	-83					**-14.7**
117	1209-1210	17454	**0.391**	0.054	0.110	0.065	0.061	-81					
120	1114	18896	**0.281**	0.055		0.075	0.058		6.4	-0.6	-11.4	**0.73811**	**-14.6**
120	1127	19713	**0.257**	0.055	0.095	0.075	0.050	-84					
120	1104	20775	**0.410**	0.056	0.108	0.070	0.060	-81					
120	1130-1140	21428	**0.383**	0.055	0.107	0.074	0.060	-80	3.6	-0.1	-15.5	**0.73980**	**-15.7**

Table S3: Summary of the chemical composition of Bay of Bengal core samples used in this work. Details can be found in the electronic appendix.

838

			LGM	Modern
	Sediment flux (t/yr)		1.10^9	1.10^9
Al/Si = 0.23	**Himalayan front**	$\overline{K/Si^*}$	0.0574 (±0.0025)	0.0574 (±0.0025)
		$\overline{H_2O^+/Si^*}$	0.1009 (±0.0068)	0.1009 (±0.0068)
	Bay of Bengal	$\overline{K/Si^*}$	0.0553 (±0.0005)	0.0510 (±0.0017)
		$\overline{H_2O^+/Si^*}$	0.1034 (±0.0075)	0.1236 (±0.0026)
		$R\phi_K$	67 (±28) %	
		$R\phi_{H2O+}$	89 (±36) %	
Al/Si = 0.21	**Himalayan front**	$\overline{K/Si^*}$	0.0524 (±0.0020)	0.0524 (±0.0020)
		$\overline{H_2O^+/Si^*}$	0.0871 (±0.0045)	0.0871 (±0.0045)
	Bay of Bengal	$\overline{K/Si^*}$	0.0499 (±0.0004)	0.0465 (±0.0014)
		$\overline{H_2O^+/Si^*}$	0.0865 (±0.0046)	0.0988 (±0.0016)
		$R\phi_K$	57 (±28) %	
		$R\phi_{H2O+}$	105 (±42) %	
Al/Si = 0.25	**Himalayan front**	$\overline{K/Si^*}$	0.0625 (±0.0029)	0.0625 (±0.0029)
		$\overline{H_2O^+/Si^*}$	0.1148 (±0.0091)	0.1148 (±0.0091)
	Bay of Bengal	$\overline{K/Si^*}$	0.0606 (±0.0006)	0.0555 (±0.0021)
		$\overline{H_2O^+/Si^*}$	0.1203 (±0.0104)	0.1484 (±0.0036)
		$R\phi_K$	73 (±32) %	
		$R\phi_{H2O+}$	84 (±33) %	

839

840 **Table S4:** Relative change in weathering fluxes exported as dissolved load to the oceans
841 obtained for K and H_2O^+ using an average Al/Si ratio of 0.23, 0.21 and 0.25. The end
842 members used for the calculation are also reported along with their uncertainty.